Vol 18 No 6, June 2009
1674-1056/2009/18(06)/2412-08

Chinese Physics B

© 2009 Chin. Phys. Soc.
and IOP Publishing Ltd

Self-consistent three-dimensional modeling and simulation of large-scale rectangular surface-wave plasma source*

Lan Chao-Hui(蓝朝晖)[a)†], Lan Chao-Zhen(蓝朝桢)[b)], Hu Xi-Wei(胡希伟)[a)], Chen Zhao-Quan(陈兆权)[a)], and Liu Ming-Hai(刘明海)[a)]

[a)] *College of Electrical and Electronic Engineering, Huazhong University of Science and Technology, Wuhan* 430074, *China*

[b)] *Institute of Surveying & Mapping, Information Engineering University, Zhengzhou* 450052, *China*

(Received 23 October 2008; revised manuscript received 25 November 2008)

A self-consistent and three-dimensional (3D) model of argon discharge in a large-scale rectangular surface-wave plasma (SWP) source is presented in this paper, which is based on the finite-difference time-domain (FDTD) approximation to Maxwell's equations self-consistently coupled with a fluid model for plasma evolution. The discharge characteristics at an input microwave power of 1200 W and a filling gas pressure of 50 Pa in the SWP source are analyzed. The simulation shows the time evolution of deposited power density at different stages, and the 3D distributions of electron density and temperature in the chamber at steady state. In addition, the results show that there is a peak of plasma density approximately at a vertical distance of 3 cm from the quartz window.

Keywords: FDTD method, surface wave plasma, fluid model
PACC: 5000, 0340K

1. Introduction

In recent years, surface wave plasma (SWP) source has been developed as a competitive processing tool for ultra-large-scale integrated (ULSI) circuit devices, flat panel displays, etc. SWP is sustained by the fields of 2.45 GHz microwaves propagating along a plasma-dielectric interface under the condition of electron density higher than the cutoff plasma density. Compared with various conventional plasma sources such as inductively-coupled plasma (ICP), capacitively-coupled plasma (CCP) and electron cyclotron resonance (ECR) devices, SWP source has many advantages,[1−4] for example, (i) no need for the use of static magnetic fields; (ii) no need for the electrodes, thus completely avoiding electrode polluting; (iii) the possibility to be enlarged to diameters larger than 0.6 m or areas larger than 0.5 m^2 (0.5×1 m^2) so as to maintain the spatial uniformity and high density ($n_e \approx 10^{11}$–10^{13} cm^{-3}) of plasma.

In practice, the large-scale spatial uniformity of plasma is the most important goal but is very difficult to achieve, only through experience (e.g. cut and try of slot antennas) may it be carried out. So we urgently need the assistance by the analysis of the theoretical model in the design of the SWP device. In this field, several research works have been done over the past ten years.[5−8] However, these works mainly focused on the cylindrical configuration of the SWP source and all the models they built were almost two-dimensional (2D). For a rectangular-type SWP source, no theoretical modeling of the discharge characteristics has been fully developed for this kind of 3D device. In Refs.[9] and [10], we built a rectangular SWP source and developed a 3D simulation code based on the assumption of spatially uniform and time-independent plasma distribution. Although this code has been used to study the wave propagation and absorption in the whole device, the simulation cannot reproduce the strong interdependence between the plasma distributions and electromagnetic wave propagation. Obviously, it is necessary to build a self-consistent 3D model for the rectangular-type SWP source. In this paper, we present a hybrid simulation employing the finite-difference time-domain (FDTD)[11] approximation to Maxwell's equations along with a fluid model for plasma evolution to study the characteristics of argon discharge in the SWP source. We intend to

*Project supported by the Special Fund of National High-Tech Development and Research Plan (Grant No 2008AA12A214).
†E-mail: lanchaohui@163.com

evaluate this model as a practical design tool for the SWP apparatus by using the simulation results.

2. Model

2.1. Configuration

Figure 1 shows the configuration of the rectangular SWP source structure, the configuration is similar to the experimental setup under operation.[9] The SWP source consists of an R22 rectangular waveguide connected to a metallic rectangular chamber with a size of 44 cm length by 22 cm width by 15 cm height. The top wall of the chamber is a quartz dielectric (a little smaller than chamber area) with a thickness of 14 mm and a relative permittivity $\varepsilon = 3.78$. Slot antennas are placed just at the bottom wall of the waveguide. The plasma is sustained through the injection of microwave energy at 2.45 GHz from the waveguide (TE_{10} mode) into the chamber.

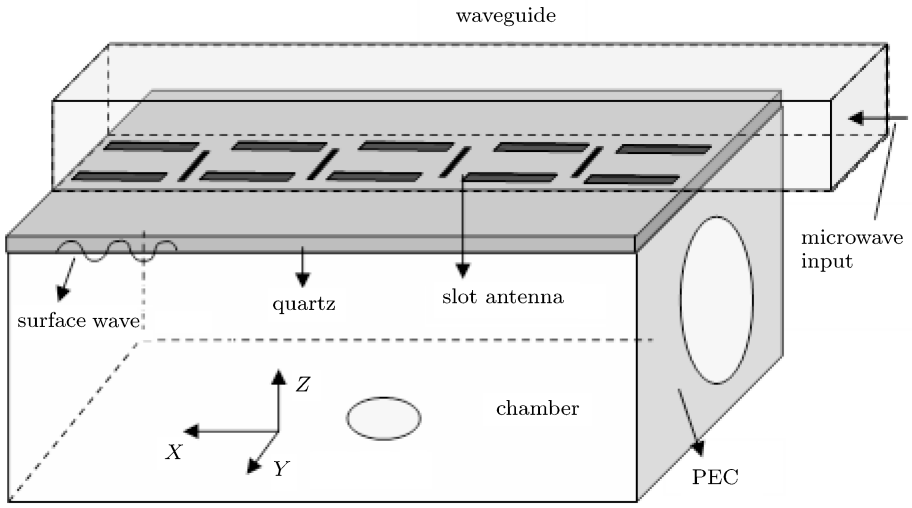


Fig.1. Three-dimensional model of the SWP source.

2.2. Physical model

The Maxwell's equations and plasma electron equations of motion are given by

$$\varepsilon \frac{\partial \boldsymbol{E}}{\partial t} = \boldsymbol{\nabla} \times \boldsymbol{H} - \boldsymbol{J}, \tag{1}$$

$$\mu \frac{\partial \boldsymbol{H}}{\partial t} = -\boldsymbol{\nabla} \times \boldsymbol{E}, \tag{2}$$

$$m_{\mathrm{e}} \frac{\partial \boldsymbol{u}}{\partial t} = -e\boldsymbol{E} - \nu_{\mathrm{en}} \boldsymbol{u}, \tag{3}$$

$$\boldsymbol{J} = -en_{\mathrm{e}} \boldsymbol{u}, \tag{4}$$

where $\boldsymbol{E}$ and $\boldsymbol{H}$ are the electric and magnetic fields, $\boldsymbol{J}$ is the plasma current density induced by microwaves, e is the electron charge, m_{e} is the mass of electron, n_{e} is the plasma electron density, v_{en} is the electron-neutral collision frequency, $\boldsymbol{u}$ is the electron velocity, μ and ε are the permeability and permittivity in free space or in quartz dielectric. Here, $\nu_{\mathrm{en}} = n_{\mathrm{n}} \sigma_{\mathrm{en}} u$ is a function of gas pressure and electron temperature, where $n_{\mathrm{n}} = p_{\mathrm{n}}/k_{\mathrm{B}} T_{\mathrm{n}}$ is the background gas density with the gas pressure p_{n}, temperature T_{n}, and Boltzmann's constant k_{B}; σ_{en} is the electron-neutral collision cross section and assumed to be constant 5×10^{-20} m^2.

The simulations are performed for a single-ionized argon plasma with the assumption of charge neutrality. Besides the ionization reaction, we also consider the excited $4s$ and $4p$ states of the argon atom. Volume ion-electron recombination is excluded, so all charge particles are lost at the walls. Because the plasma in the present study has a low degree of ionization, the momentum transfer between electrons and ions is much smaller than that between electrons and neutrals. Therefore, we neglect the momentum transfer between electrons and ions. In the microwave

plasma, there may exist some collisionless mechanisms of energy absorption such as statistical heating and Landau damping, but we neglect these heating mechanisms and only consider the Joule heating by the microwave. On the basis of these assumptions, the electron fluid continuity and energy balance equations in plasma can be written as

$$\frac{\partial n_{\rm e}}{\partial t} + \boldsymbol{\nabla}\cdot\boldsymbol{\Gamma}_{\rm e} = K_{\rm i} n_{\rm e} n_{\rm n}, \tag{5}$$

$$\frac{\partial}{\partial t}\left(\frac{3}{2} n_{\rm e} k_B T_{\rm e}\right) + \boldsymbol{\nabla}\cdot\boldsymbol{q}_{\rm e} = P_{\rm abs} - P_{\rm coll}, \tag{6}$$

where

$$\boldsymbol{\Gamma}_{\rm e} = -\mu_{\rm e} n_{\rm e} \boldsymbol{E}_{\rm amb} - \frac{k_{\rm B}}{m_{\rm e}\nu_{\rm en}}\boldsymbol{\nabla}\left(n_{\rm e} T_{\rm e}\right) \tag{7}$$

is the electron flux expression from the electron momentum balance, and

$$\boldsymbol{q}_{\rm e} = \frac{5}{2}\boldsymbol{\Gamma}_{\rm e} k_{\rm B} T_{\rm e} - \frac{5 n_{\rm e} k_{\rm B} T_{\rm e}}{2 m_{\rm e}\nu_{\rm en}}\boldsymbol{\nabla} k_{\rm B} T_{\rm e} \tag{8}$$

is the electron energy flux; $\mu_{\rm e}$ is the electron mobility, $P_{\rm abs} = \boldsymbol{J}\cdot\boldsymbol{E}$ is the energy deposited into electrons. The fluid equations (5)–(8) are derived by assuming an isotropic electron energy distribution function (EEDF). We know the possibility of anisotropic electron energies, but we neglect this effect in this study. Because we take into account only the ionization and the excitation of the $4s$ and $4p$ states of the argon atom, the power density of energy losses due to electron-neutral inelastic collisions can thus be expressed as

$$P_{\rm coll} = n_{\rm e} n_{\rm n} K_{\rm i} U_{\rm i} + n_{\rm e} n_{\rm n} K_{4s} U_{4s} + n_{\rm e} n_{\rm n} K_{4p} U_{4p}, \tag{9}$$

where K_i, K_{4s} and K_{4p} denote the rate coefficients for ionization and excitation. We use Eqs.(10)–(12) as the rate coefficients as presented by Ashida[12]

$$K_i = 2.3\times10^{-14} T_{\rm eV}^{0.68} \exp\left(-U_i/T_{\rm eV}\right), \tag{10}$$

$$K_{4s} = 5.0\times10^{-15} T_{\rm eV}^{0.74} \exp\left(-U_{4s}/T_{\rm eV}\right), \tag{11}$$

$$K_{4p} = 1.4\times10^{-14} T_{\rm eV}^{0.71} \exp\left(-U_{4p}/T_{\rm eV}\right), \tag{12}$$

where $U_{\rm i} = 15.76$ eV, $U_{4s} = 11.5$ eV and $U_{4p} = 13.2$ eV are the respective threshold energies for ionization and excitation of the states $4s$ and $4p$. $T_{\rm eV}$ is the electron temperature and the unit is electron volt.

The electrostatic field in Eq.(7) is

$$\boldsymbol{E}_{\rm amb} = \frac{D_{\rm i} - D_{\rm e}}{\mu_{\rm e} + \mu_{\rm i}}\cdot\frac{\boldsymbol{\nabla} n_{\rm e}}{n_{\rm e}} - \frac{1}{\mu_{\rm e} + \mu_{\rm i}}\frac{k_{\rm B}\boldsymbol{\nabla} T_{\rm e}}{m_{\rm e}\nu_{\rm en}}, \tag{13}$$

which can be derived from the assumption of ambipolar diffusion $\boldsymbol{\Gamma}_{\rm e} = \boldsymbol{\Gamma}_{\rm i}$ with the ion flux

$$\boldsymbol{\Gamma}_{\rm i} = \mu_{\rm i} n_{\rm i} \boldsymbol{E}_{\rm amb} - \frac{k_{\rm B}}{m_{\rm i}\nu_{\rm in}}\boldsymbol{\nabla}\left(n_{\rm i} T_{\rm i}\right), \tag{14}$$

where $m_{\rm i}$, $T_{\rm i}$ and $n_{\rm i}$ are the mass, temperature and density of ion respectively; and $n_{\rm i} \approx n_{\rm e}$ due to charge neutrality. In Eqs.(7), (13) and (14), $\mu_\alpha = e/m_\alpha\nu_{\alpha n}$ $(\alpha = e, i)$ are the electron and ion mobilities, and $D_\alpha = k_{\rm B} T_\alpha/m_\alpha\nu_{\alpha n} (\alpha = i, e)$ are the electron and ion diffusion constants, where $\nu_{\rm in} = \sigma_{\rm in}\bar{v}_{\rm i} n_{\rm n}$ is the ion-neutral momentum transfer collision frequency. Here, we have $\sigma_{\rm in} = 5\times10^{-19}$ m^2 for the corresponding collision cross section, and $T_i = 0.05$ eV to specify the ion thermal speed $\bar{v}_{\rm i} = \left(8k_{\rm B} T_{\rm i}/\pi m_{\rm i}\right)^{1/2}$. The ion temperature are assumed to be spatially uniform, hence $\nabla T_{\rm i} = 0$.

The plasma electron density and temperature in Eqs.(5) and (6) can be calculated numerically with a time increment $\Delta t_{\rm fluid}$, which is usually far greater than the time increment $\Delta t_{\rm FDTD}$ of Eqs.(1)–(5) when using the FDTD method as the solver of Maxwell's equations. So within several periods of microwave, the plasma electron density and temperature can be viewed as in quasi-steady-state $(\partial/\partial t = 0)$ in comparison to the time scale of the microwave oscillation. Then equations (5) and (6) can be reduced to

$$\boldsymbol{\nabla}\cdot\boldsymbol{\Gamma}_{\rm e} = K_{\rm i} n_{\rm e} n_{\rm n}, \tag{15}$$

$$\boldsymbol{\nabla}\cdot\boldsymbol{q}_{\rm e} = P_{\rm abs} - P_{\rm coll}, \tag{16}$$

which are solved by finite differences. From Eqs.(7), (8) and (13), the left-hand sides of the above two equations can be written as

$$\begin{aligned}\boldsymbol{\nabla}\cdot\boldsymbol{\Gamma}_{\rm e} = &-\frac{\mu_{\rm e} D_{\rm i} + \mu_{\rm i} D_{\rm e}}{\mu_{\rm e} + \mu_{\rm i}}\nabla^2 n_{\rm e} - \frac{\mu_{\rm i}}{\mu_{\rm e} + \mu_{\rm i}}\frac{k_{\rm B} n_{\rm e}}{m_{\rm e}\nu_{\rm en}}\nabla^2 T_{\rm e}\\ &- \frac{2\mu_{\rm i}}{\mu_{\rm e} + \mu_{\rm i}}\frac{k_{\rm B}}{m_{\rm e}\nu_{\rm en}}\nabla n_{\rm e}\cdot\nabla T_{\rm e},\end{aligned} \tag{17}$$

$$\begin{aligned}\boldsymbol{\nabla}\cdot\boldsymbol{q}_{\rm e} = &-\frac{5}{2}\left(1 + \frac{\mu_{\rm i}}{\mu_{\rm e} + \mu_{\rm i}}\right) n_{\rm e} k_{\rm B} D_{\rm e}\nabla^2 T_{\rm e}\\ &- \frac{5}{2}\frac{\mu_{\rm e} D_{\rm i} + 4\mu_{\rm i} D_{\rm e} + \mu_{\rm e} D_{\rm e}}{\mu_{\rm e} + \mu_{\rm i}} k_{\rm B}\nabla n_{\rm e}\cdot\nabla T_{\rm e}\\ &- \frac{5}{2}\frac{\mu_{\rm e} D_{\rm i} + \mu_{\rm i} D_{\rm e}}{\mu_{\rm e} + \mu_{\rm i}} k_{\rm B} T_{\rm e}\nabla^2 n_{\rm e}\\ &- \frac{5}{2}\left(1 + \frac{\mu_{\rm i}}{\mu_{\rm e} + \mu_{\rm i}}\right)\frac{k_{\rm B}^2 n_{\rm e}}{m_{\rm e}\nu_{\rm en}}\nabla T_{\rm e}\cdot\nabla T_{\rm e}.\end{aligned} \tag{18}$$

The period-averaged electromagnetic deposited power density in Eq.(16) is given by

$$P_{\rm abs} = \frac{1}{T}\int_t^{t+T} \boldsymbol{J}\cdot\boldsymbol{E}{\rm d}t, \tag{19}$$

where $T(\approx 0.408$ ns) is the period of 2.45 GHz microwave.

The Maxwell's equations (1) and (2) are solved by using the FDTD method, while the motion equation (3) is discretized by the auxiliary differential equation (ADE) method.[13] For the FDTD boundary conditions, all conducting surfaces (metal walls) are assumed to be perfect electrical conductors (PEC), i.e., the tangential electric-field components on these planes are forced to be zero. At the right end of waveguide (not shown in Fig.1), 14 cells perfectly matched layer (PML)[11] is designed to absorb the reflected waves. The boundary conditions for Eqs.(15) and (16) are

$$\Gamma_{e\perp} = n_e u_B = 0.605 n_e \sqrt{k_B T_e / m_i}, \tag{20}$$

$$q_{e\perp} = k_B T_e \left(2.5 + \ln \sqrt{m_i / 2\pi m_e}\right) \Gamma_{e\perp}, \tag{21}$$

where $\Gamma_{e\perp}$ and $q_{e\perp}$ are the respective components of $\boldsymbol{\Gamma}_e$ and $\boldsymbol{q}_e$ perpendicular to the walls, u_B is the Bohm velocity. Here we assume that there is a plasma sheath at the plasma-wall interface where the plasma contacts metal wall or quartz window.

2.3. Method for calculation

In the algorithm we use for the FDTD/fluid hybrid simulation, as shown in Fig.2, there are two subloops within the main loop: one is called the FDTD subloop (left-hand part), and the other is called the plasma fluid subloop (right-hand part). The two subloops are head-tail connected as a successive main loop. At the beginning of one calculation, electron density and temperature in the whole chamber are initialized to be constants, i.e., $T_0 = 2$ eV, $n_{e0} = 10^{18}$ m^{-3}. By performing the FDTD simulations of Eqs.(1)–(4), we obtain the steady-state electromagnetic field in 15–25 microwave periods. The first step can also be seen as a spatially uniform and time-independent plasma model of SWP, the detailed description of the simulation of this model can be found in our other paper.[10] After the steady state has been achieved, we calculate Eq.(19) to obtain the spatial distribution of deposited power, which as an input is transferred to plasma fluid subloop to solve for the electron density and temperature. Typically in 1750–2000 Gauss–Siedel iterations, a converged solution of the electron density and temperature is reached. Then we use the electron density and temperature obtained as the input of the FDTD subloop. By reciprocally iterating of these two subloops, the main loop reaches a converged solution in approximately 10–15 iterations.

The numerical convergence was checked by performing several simulations, and no large time-scale variations of the plasma parameters were observed when using simulations with a large number of iterations times. It is further noted that the final converged state of plasma depends on the input microwave power P_{in} and the given gas pressure p_n, but not on the initial values or distributions of electron density n_e and electron temperature T_e.

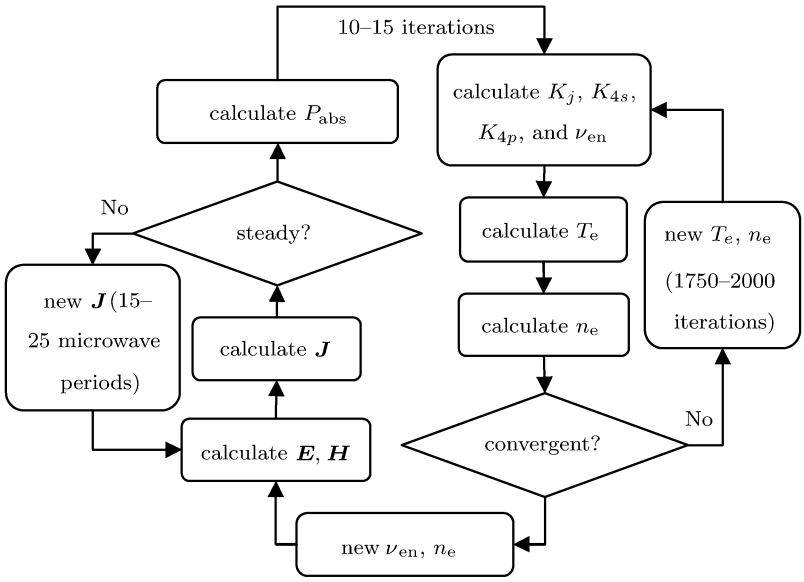


Fig.2. Numerical model iteration scheme.

3. Results and discussion

In the following calculations, the discharge characteristics of the SWP source are simulated at a pressure of 50 Pa. The nominal input microwave power for this simulation is 1200 W at a frequency of 2.45 GHz. In the simulation, the time increment for FDTD is taken to be $\Delta t_{\mathrm{FDTD}} = 3.08 \times 10^{-12}$ s, and the iteration times for FDTD and the Gauss–Siedel method in every main loop are taken to be 2000 (about 15 periods of wave) and 1750, respectively. After 8^{th} main loop iteration, the plasma parameters in the chamber and the electromagnetic field in the whole device tend to become stable. It is noted that a larger number of main loop iteration times are needed for lower input microwave powers.

Figures 3(a)–3(f) show the time evolution of the 3D distribution of deposited power density, corresponding to the $2{\sim}7^{\mathrm{th}}$ main loop iterations respectively. These figures can also be viewed as the different states of surface deposited power density at different

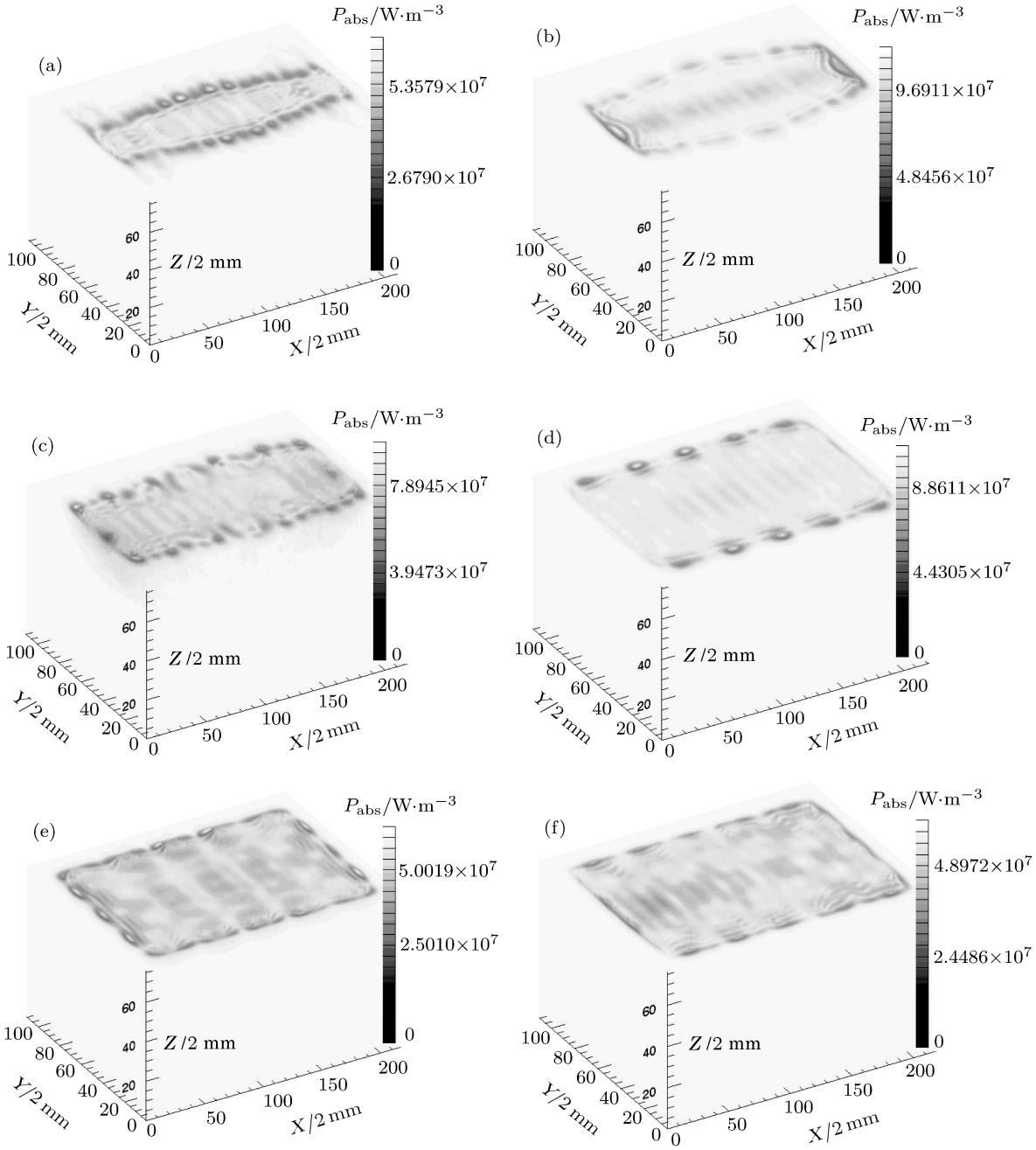


Fig.3. Time evolution of deposited power density (W/m^3) distribution in 3D space, (a)–(f) respectively represent the $2{\sim}7^{\mathrm{th}}$ main loop iterations ($P_{\mathrm{in}} = 1200$ W, $p_{\mathrm{n}} = 50$ Pa).

times. At the beginning, because the electron density is relatively low, the deposited power is concentrated in a narrow area just at the bottom of the waveguide as shown in Fig.3(a), leading to a nonuniform distribution of electron density. The deposited power density can easily and uniformly spread out in the x direction, for which there is a precondition: the powers injected into the chamber through each slot antenna are high and uniform enough. In order to achieve this, in Fig.1 we placed the slot antennas periodically along the x direction just at the positions where the magnetic field can reach the wave crest of the standing wave. Because the length of the chamber is not too big, here we do not consider the influence of slotting on the standing waves in the waveguide, which actually is a main factor that should be taken into account in the design of a larger SWP device. In Figs.3(b)–3(d), one can see that with the increase of time, the surface deposited power density starts to spread out towards the entire width of the quartz window. In this process, the fringe-deposited power is much bigger than that in the inner region, producing a bigger electron density in the periphery and forming a density concavity in the inner part. This distribution of electron density may be in favor of the absorption of microwave power and thus in favor of the outspread of electron density. In Figs.3(e)–3(f), the deposited power density completely spreads out and covers the whole quartz window. It is interesting to note that the whole process is totally spontaneous, and only depends on external conditions such as input power, gas pressure and the structure of slot antennas.

Figure 4 shows the snapshot of the surface wave (E_z field) pattern near the plasma-quartz interface, which corresponds to the deposited power density shown in Fig.3(f). The darker parts represent more intense electromagnetic fields. One can see that the pattern in Fig.4 is not so uniform as the corresponding deposited power density, but they are not contradictory because figure 4 is just a snapshot, and the mode in the pattern is not an eigen-mode, thus the actual pattern is dynamic variable and the dark parts will keep moving around. On the other hand, the strong correlation between the surface wave pattern and the structure of slot antennas can be found in this figure. Different forms of slot antennas will lead to totally different distributions of fields and plasma parameters.

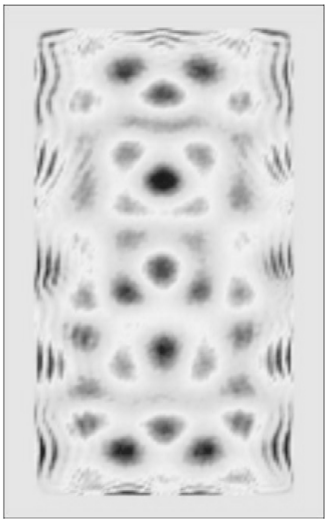


Fig.4. Snapshot of the surface wave (E_z field) pattern near the plasma-quartz interface. Note that the area of the quartz window is smaller than that of the chamber.

Figures 5 and 6 show respectively the 3D distributions of the electron density n_e and temperature T_e in the entire chamber. According to the physical model, on the one hand, plasma absorbs surface power leaking from the slot antennas and carried by the surface wave propagating along the plasma-quartz interface; on the other hand, the energy and charged particles of the plasma are lost at the walls through diffusion. When these two factors are balanced, the stable distributions of n_e and T_e can be achieved. From Eqs.(15) and (16), the distribution of deposited power density directly determines that of T_e and thereby determines that of n_e. So it can be clearly seen from Fig.6 that the upper surface distribution of T_e is quite similar to that shown in Fig.3(f). Because the deposited power is very uniform under the quartz window, the upper surface distribution of n_e and T_e are also comparatively uniform, forming a platform of n_e at the top of the chamber. In fact, the distribution of deposited power density is not completely uniform under the quartz window, however, the n_e can keep relatively uniform through diffusion throughout the chamber. In addition, comparing Fig.5 with Fig.6, one can see that the T_e of bulk plasma is much more uniform than n_e, especially at the positions near the bottom wall and the corners of the chamber.

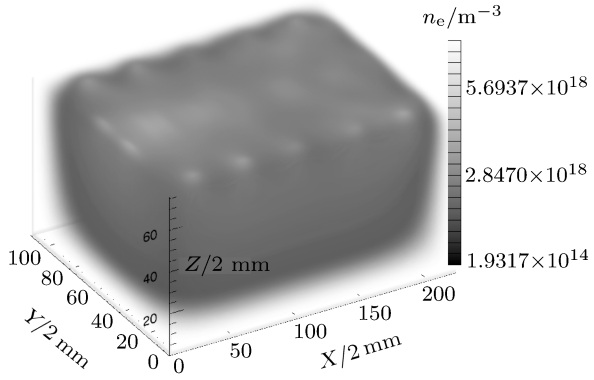


Fig.5. Electron density in 3D distribution.

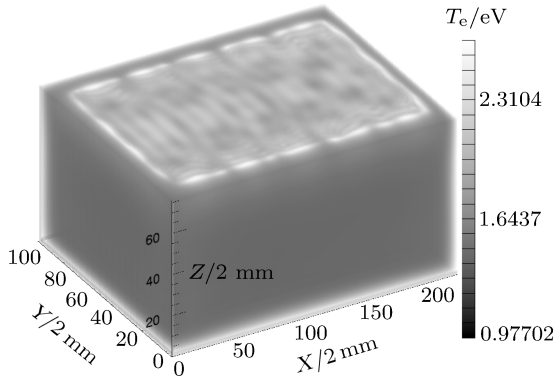


Fig.6. Electron temperature in 3D distribution.

Figure 7 shows the n_e and T_e distributions along the vertical central axis of the rectangular chamber. For an injected microwave power $P_{in} = 1200$ W and a gas pressure $p_n = 50$ Pa, the maximal values of n_e and T_e can reach about 6×10^{18} m^{-3} and 2 eV respectively. The distributions of n_e and T_e are nonuniform in the z direction due to diffusion, and the distribution of n_e has a peak at around $z = 12$ cm or a vertical distance of 3 cm from the quartz window. From $z = 12$ cm to $z = 15$ cm, the distribution of T_e is quite different from that of n_e: the former rises monotonously and steeply

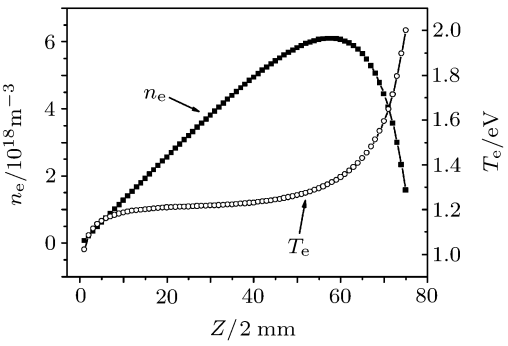


Fig.7. Electron density and temperature distributions along the vertical central axis of the chamber.

while the latter drops down rapidly after reaching its peak. This is the reason that figure 6 looks so bright while figure 5 looks so dark on the upper surface.

Figure 8 shows the horizontal distributions of n_e and T_e, the sampled line is located at a vertical distance of 1.2 cm from the quartz window. The average derivations of n_e and T_e in the platform area (x=5–40 cm) are no more than 1.0×10^{18} m^{-3} and 0.1 eV, respectively. With the increase of the distance, the ripples of n_e and T_e in the platform area will rapidly weaken after reaching their respective maximum. It is necessary to note that the n_e curve in Fig.8 does not exhibit bilateral symmetry, i.e. the values on the left side are slightly higher than those on the right side. The reason may be that the slots close to the microwave source can better radiate powers than those far from the microwave source.

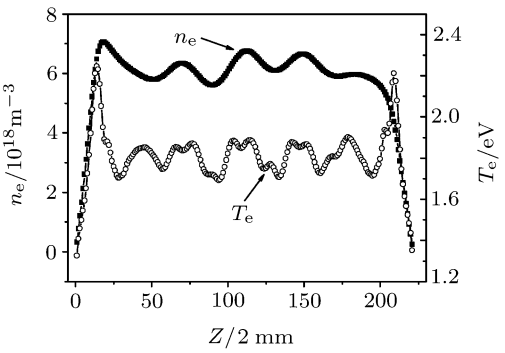


Fig.8. Horizontal distributions of electron density and temperature, the sampled lines are located at vertical distances of 1.2 cm and 2 mm from the quartz window.

4. Summary

We have presented a self-consistent and full-scale three-dimensional FDTD/fluid hybrid model for the large-scale rectangular surface wave source. The hybrid model employs the FDTD method to solve the electromagnetic equations and at the same time employs a plasma fluid model to self-consistently obtain steady-state plasma spatial distributions. A detailed description of the algorithm has also been presented. In order to evaluate whether the simulation model is applicable to reproduce the characteristic spatial profiles of the electron density and temperature, we have simulated the time evolution of the argon surface-wave discharge at an input microwave power of 1200 W and a gas pressure of 50 Pa. The results show that the electron density has such a characteristic profile that the peak is located several centimeters from the bound-

ary, while the electron temperature monotonously increases towards the boundary. The tendencies and the orders of magnitudes of the results obtained are in good agreement with existing experimental data. Further investigations are now in progress to validate the FDTD/fluid hybrid simulation by comparing the numerical results with experimental investigations.

References

[1] Ghanashev I and Sugai H 2000 *Phys. Plasmas* **7** 3051
[2] Ganashev I, Nagatsu M and Sugai H 1997 *Jpn. J. Appl. Phys.* **36** 337
[3] Sugai H, Ghanashev I and Nagatsu M 1998 *Plasma Sources Sci. Technol.* **7** 192
[4] Liu M H, Sugai H, Hu X W, Ishijima T, Jiang Z H, Li B and Dan M 2006 *Acta Phys. Sin.* **55** 5905 (in Chinese)
[5] Kousaka H and Ono K 2002 *Jpn. J. Appl. Phys.* **41** 2199
[6] Chen Q, Aoyagi H P and Katsurai M 1999 *IEEE Trans. Plasma Science* **27** 164
[7] Tatarova E, Dias F M and Ferreira C M 1998 *J. Appl. Phys.* **83** 4602
[8] Tatarova E, Dias F M, Henriques J and Ferreira C M 2005 *IEEE Trans. Plasma Science.* **33** 866
[9] Chen Z Q, Zhou P Q, Chen W, Lan C H, Liu M H and Hu X W 2008 *Plasma Sci. Technol.* **10** 655
[10] Lan C H, Chen Z Q, Liu M H and Hu X W 2009 *Plasma Sci. Technol.* **11** 66
[11] Taflove A 1995 *Computational Electrodynamics: the Finite-Difference Time-Domain Method* (Boston: Artech House)
[12] Ashida S, Lee C and Lieberman M A 1995 *J. Vac. Sci. Technol.* A **13** 2498
[13] Kashiwa T and Fukai I 1990 *Microwave Opt. Technol. Lett.* **3** 203